

Emergent Topology in Many-Body Dissipative Quantum Chaos

Antonio M. García-García,^{1,*} Lucas Sá,^{2,3,†} Jacobus J. M. Verbaarschot,^{4,‡} and Can Yin^{1,§}

¹*Shanghai Center for Complex Physics, School of Physics and Astronomy,
Shanghai Jiao Tong University, Shanghai 200240, China*

²*TCM Group, Cavendish Laboratory, University of Cambridge, JJ Thomson Avenue, Cambridge CB3 0HE, UK*

³*CeFEMA, Instituto Superior Técnico, Universidade de Lisboa, Av. Rovisco Pais, 1049-001 Lisboa, Portugal*

⁴*Center for Nuclear Theory and Department of Physics and Astronomy,
Stony Brook University, Stony Brook, New York 11794, USA*

(Dated: December 7, 2023)

The identification, description, and classification of topological features is an engine of discovery and innovation in several fields of physics. This research encompasses a broad variety of systems, from the integer and fractional Chern insulators in condensed matter, to protected states in complex photonic lattices in optics, and the structure of the QCD vacuum. Here, we introduce another playground for topology: the dissipative dynamics of the Sachdev-Ye-Kitaev (SYK) model, N fermions in zero dimensions with strong q -body interactions coupled to a Markovian bath. For $q = 4, 8, \dots$ and certain choices of N and bath details, involving pseudo-Hermiticity, we find a rectangular block representation of the vectorized Liouvillian that is directly related to the existence of an anomalous trace of the unitary operator implementing fermionic exchange. As a consequence of this rectangularization, the Liouvillian has purely real modes for any coupling to the bath. Some of them are demonstrated to be topological by an explicit calculation of the spectral flow, leading to a symmetry-dependent topological index ν . Topological properties have universal features: they are robust to changes in the Liouvillian provided that the symmetries are respected and they are also observed if the SYK model is replaced by a quantum chaotic dephasing spin chain in the same symmetry class. Moreover, the topological symmetry class can be robustly characterized by the level statistics of the corresponding random matrix ensemble. In the limit of weak coupling to the bath, topological modes govern the approach to equilibrium, which may enable a direct path for experimental confirmation of topology in dissipative many-body quantum chaotic systems.

I. INTRODUCTION

Nontrivial topological features in wave functions and gauge configurations have helped explain a broad variety of physical phenomena in different research areas. The anomalous decay of the neutral pion into two photons due to the chiral anomaly [1, 2] has its origin [3, 4] in certain topologically nontrivial gauge configurations of zero field strength in which fermions have zero modes. The Atiyah-Singer index theorem [5] then relates the number of the fermionic zero modes with a topological invariant of the gauge fields. Later, these ideas played an important role in the development of effective models of the QCD vacuum aimed at explaining the phenomenon of spontaneous chiral symmetry breaking [6], and also in the proposal of the chiral random matrix ensembles [7, 8] that capture universal properties of the QCD Dirac operator. In condensed matter, the experimental discovery [9] of the quantization of the Hall conductivity and its theoretical explanation [10] based on the existence of topologically protected edge states triggered an enormous interest in topological quantum matter. Highlights of this endeavor include the discovery [11] and theoretical explanation [12] of the fractional quantum Hall effect caused by strong electronic interactions in two dimensions and the theoretical prediction [13], and experimental confirmation [14], of topological features without the need of a magnetic field, the so-called spin-Hall effect [15–17].

The realization that, in momentum space, topology

only requires a certain symmetry in the band structure of the material, which depends strongly on the dimensionality, and the existence of a gap in the spectrum that protects the edge states led to the proposal [18–21], and experimental confirmation [22], of topological insulators in three dimensions. Such ideas were also applied to the characterization of topological superconductors [23], and the employment of K-homology techniques led to a full characterization of topological insulators and superconductors [24–26] based on symmetry and dimensionality. In this context, interactions can, in some cases [27], change the nature of the topological invariants [27]. Topology has also been intensively investigated in non-Hermitian Hamiltonians or Liouvillians in condensed matter and cold atom [28–40], in the context of QCD Wilson fermions [41–45], and in random matrix theory [45–53], while quantum optical settings [36] are an adequate experimental platform to simulate non-Hermitian topology. In condensed matter and cold atoms, most of the research [28, 32] has focused on non-interacting systems with an emphasis on comparing with the previously mentioned classification of non-interacting topological insulators by using, for instance, Hermitization techniques. Preliminary studies of the role of interactions and topology in non-Hermitian systems [54, 55], employing the interacting Hatano-Nelson model [56, 57] and Liouvillians with two-body losses [58], point to profound differences with respect to the non-interacting limit [59] that call for new ideas and techniques.

In this paper, we propose a novel platform to study

non-Hermitian topology in strongly interacting systems: the dissipative dynamics of the Sachdev-Ye-Kitaev (SYK) model [60–66] coupled to a Markovian bath [67–71]. We find, through an explicit calculation of the topological index ν , that the vectorized Liouvillian has ν purely real topological modes for certain choices of $q/2$ even, N , and bath details, leading to four new topological universality classes. We start our analysis with the definition of the model and the description of its symmetries.

II. MODEL AND SYMMETRIES

We study the SYK model of N Majoranas $\psi_i = \psi_i^\dagger$, $i = 1, 2, \dots, N$, with q -body interactions of infinite range in zero dimensions, whose Hamiltonian is given by

$$H = -i^{\frac{q}{2}} \sum_{1 \leq i_1 < i_2 < \dots < i_q \leq N} K_{i_1 i_2 \dots i_q} \psi_{i_1} \psi_{i_2} \dots \psi_{i_q}, \quad (1)$$

where $\{\psi_i, \psi_j\} = \delta_{ij}$, $K_{i_1 i_2 \dots i_q}$ are Gaussian random couplings with zero average and variance $2^{q-1}(q-1)/(qN^{q-1})$, N is even and q is a multiple of four. We are mainly interested in the dynamics of this SYK coupled to a Markovian bath, characterized by jump operators $L_{i_1 i_2 \dots i_r} = i^{r(r-1)/2} \psi_{i_1} \psi_{i_2} \dots \psi_{i_r}$, described by the time evolution of the density matrix ρ ,

$$\begin{aligned} \frac{d\rho}{dt} = \mathcal{L}(\rho) &\equiv -i[H, \rho] + \lambda \frac{N^{1-r}}{r} \\ &\times \sum_{1 \leq i_1 < \dots < i_r \leq N} \left(L_{i_1 \dots i_r} \rho L_{i_1 \dots i_r}^\dagger - \frac{1}{2} \{L_{i_1 \dots i_r}^\dagger L_{i_1 \dots i_r}, \rho\} \right), \end{aligned} \quad (2)$$

where \mathcal{L} stands for the Liouvillian (of Lindblad form) and λ denotes the dissipation strength. After the necessary vectorization to set up the path integral on the Keldysh contour, with branches denoted by $+$ and $-$, namely $\psi_k \rho \rightarrow \psi_k^+ |\rho\rangle$ and $\rho \psi_k \rightarrow i\psi_k^- |\rho\rangle$, where $|\rho\rangle = \sum_{ij} \langle i|\rho|j\rangle |i\rangle|j\rangle$ is the vectorized density matrix, the vectorized Liouvillian is given by,

$$\mathcal{L} = -iH_+ + iH_- + \lambda H_I, \quad (3)$$

where $H_{+,-}$ are obtained from the single-site SYK Hamiltonian in Eq. (1) by replacing $\psi_k \rightarrow \psi_k^{+,-}$ with identical couplings for $H_+ = H \otimes \mathbf{I}$ and $H_- = \mathbf{I} \otimes H$ with \mathbf{I} the identity matrix while

$$H_I = i^r \frac{N^{1-r}}{r} \lambda \sum_{1 \leq i_1 < \dots < i_r \leq N} \psi_{i_1}^+ \dots \psi_{i_r}^+ \psi_{i_1}^- \dots \psi_{i_r}^- \quad (4)$$

describes the effect of the bath. For the sake of simplicity, we drop the constant term $-\lambda N^{1-r} 2^{-r} \binom{N}{r}/r$ in Eq. (4). For later use, we define $H_0 = -iH_+ + iH_-$. We note that the Liouvillian above has been recently [72] employed in

a symmetry classification of many-body quantum chaotic systems in contact with a Markovian bath.

For reasons that will become apparent shortly, our interest is focused on values of N , q , and r in Eqs. (3) and (4) that lead to a pseudo-Hermitian Liouvillian, $Q\mathcal{L}^\dagger = \mathcal{L}Q$, where

$$Q = \exp \left\{ -\frac{\pi}{4} \sum_{i=1}^N \psi_i^+ \psi_i^- \right\} = \prod_{i=1}^N \frac{1}{\sqrt{2}} \left(1 - 2\psi_i^+ \psi_i^- \right), \quad (5)$$

is a unitary operator that commutes (anti-commutes) with H_0 (H_I) and satisfies $Q^4 = \mathbf{I}$, i.e., has eigenvalues ± 1 and $\pm i$. Up to a sign, Q exchanges Majoranas labeled by the $+$ and $-$ contours: $Q\psi_i^+ Q^{-1} = \psi_i^-$, $Q\psi_i^- Q^{-1} = -\psi_i^+$. In a recent classification of PT-symmetric systems [73], we found four of these pseudo-Hermitian classes: AIII_ν , BDI_ν^\dagger , $\text{CI}_{-\nu}$, and $\text{BDI}_{+\nu}$; see Table I for details.

A key feature of these classes is the emergence of rectangular blocks of the SYK Liouvillian in sectors of good quantum numbers. To see this, we define the single-site fermionic parities,

$$\begin{aligned} S_+ &= 2^{N/2} i^{N(N-1)/2} \prod_{i=1}^N \psi_i^+, \\ S_- &= 2^{N/2} i^{N(N+1)/2} \prod_{i=1}^N i\psi_i^-, \end{aligned} \quad (6)$$

and the total fermionic parity $S = S_+ S_-$. The Liouvillian block diagonalizes in a basis spanned by S for odd r and by S_+ and S_- for even r . Each of these blocks has additional substructure because of the commutation properties of Q with H_0 and H_I (we emphasize that Q and \mathcal{L} do not commute): in the basis in which Q is diagonal, H_I is block diagonal, while H_0 is block anti-diagonal (i.e., H_I connects states with the same eigenvalue of Q , while H_0 connects states with $Q = +1$ to states with $Q = -1$). In blocks with $S = +1$, corresponding to the sector of Q with eigenvalues ± 1 , the trace of Q (projected onto S for odd r , or onto S_+ and S_- for even r), denoted by ν , is nonzero, $\nu = \text{Tr } \mathbb{P}_S^{+1} Q = 2^{N/2}$ (odd r), and $\nu = \text{Tr } \mathbb{P}_+^{+1} \mathbb{P}_+^{+1} Q = 2^{N/2}/2$ (even r). This has the remarkable consequence that the two diagonal blocks (corresponding to the two sectors of H_I with $Q = \pm 1$, respectively) have different dimensions, n and $n + \nu$ (with $2n + \nu = 2^N/2$ for odd r and $2n + \nu = 2^N/4$ for even r), and the off-diagonal blocks (corresponding to H_0 and connecting states $Q = +1$ with $Q = -1$) become *rectangular* $n \times (n + \nu)$ matrices, see Table I. At $\lambda = 0$, each sector of \mathcal{L} is thus block anti-diagonal with rectangular blocks and has, therefore, ν zero modes. For finite λ , the pseudo-Hermiticity implies that the zero modes become purely real modes, as shown in Ref. [52] for a matrix with the block structure of AIII_ν (see Table I).

The existence of rectangular blocks for the pseudo-

Table I. Rectangular block representation of the SYK Liouvillian Eq. (3) for pseudo-Hermitian classes AIII $_{\nu}$, BDI $_{\nu}^{\dagger}$, BDI $_{++\nu}$ and CI $_{--\nu}$. In the second column, we give the block structure [73], where the diagonal blocks have different sizes, namely, A is $(n + \nu) \times (n + \nu)$ and D is $n \times n$, while the off-diagonal blocks are rectangular, namely, B is $(n + \nu) \times n$ and C is $n \times (n + \nu)$. For each class, we also list the parity of $N/2$ and r , the quantum numbers of the block with nonzero index $\text{Tr } \mathbb{P}Q = \nu$ and the RMT universality class of the level statistics of the real topological modes. We stress that in all cases $q/2$ is even as this is a necessary condition for topology.

Class	Rectangular Blocks and symmetries		SYK (λ small)				
	Matrix structure	Symmetry operator	$(-1)^{\frac{N}{2}}$	$(-1)^r$	Block	ν	RMT
AIII $_{\nu}$	$\begin{pmatrix} A & B \\ -B^{\dagger} & D \end{pmatrix}$, $A = A^{\dagger}$, $D = D^{\dagger}$	$\mathcal{Q}_z = \sigma_z$	-1	+1	$S_+ S_- = 1$	$2^{\frac{N}{2}-1}$	GUE
BDI $_{\nu}^{\dagger}$	$\begin{pmatrix} A & B \\ -B^{\dagger} & D^* \end{pmatrix}$, $A = A^{\top} = A^{\dagger}$, $B = B^*$, $D = D^{\top} = D^{\dagger}$	$\mathcal{T}_+ = K$, $\mathcal{C}_+ = \sigma_z K$	+1	+1	$S_+ S_- = 1$	$2^{\frac{N}{2}-1}$	GOE
BDI $_{++\nu}$	$\begin{pmatrix} A & B \\ A^{\top} & C^{\top} \\ B^{\top} & D^{\top} \end{pmatrix}$, $A = A^*$, $B = -B^*$, $C = -C^*$, $D = D^*$	$\mathcal{T}_+ = (I \otimes \sigma_z)K$, $\mathcal{T}_- = (\sigma_z \otimes \sigma_z)K$, $\mathcal{C}_+ = K$, $\mathcal{C}_- = (\sigma_z \otimes I)K$	+1	-1	$S = 1$	$2^{\frac{N}{2}}$	BDI
CI $_{--\nu}$	$\begin{pmatrix} 0 & 0 & A & B \\ 0 & 0 & -B^{\top} & D \\ A^* & B^* & 0 & 0 \\ -B^{\dagger} & D^* & 0 & 0 \end{pmatrix}$, $A^{\top} = A$, $D^{\top} = D$	$\mathcal{T}_+ = (\sigma_x \otimes I)K$, $\mathcal{T}_- = (i\sigma_y \otimes I)K$, $\mathcal{C}_+ = (\sigma_x \otimes \sigma_z)K$, $\mathcal{C}_- = (i\sigma_y \otimes \sigma_z)K$	-1	-1	$S = 1$	$2^{\frac{N}{2}}$	CI

Hermitian Liouvillian Eq. (3), closely related to the anomalous trace of the operator Q , $\text{Tr } \mathbb{P}Q = \nu$, suggests the existence of topological features. We now show explicitly that the finite trace of Q is indeed a topological invariant by an explicit calculation of the spectral flow of the eigenvalues of $Q(\mathcal{L} + mI)$ with \mathcal{L} the vectorized Liouvillian Eq. (3) and m a real parameter that characterizes the flow.

III. ANALYTIC CALCULATION OF THE TOPOLOGICAL INDEX

We compute the index from the spectral flow of the m -deformed Liouvillian Eq. (3),

$$\tilde{\mathcal{L}}(m) = H_0 + \lambda H_I + mI, \quad (7)$$

where m is real. We assume that $\tilde{\mathcal{L}}(m)$ has been projected, denoted below by the projection operator \mathbb{P} , into a sector with fixed quantum numbers, namely, $S = +1$ or $S_+ = S_-$. $\tilde{\mathcal{L}}$ is pseudo-Hermitian (i.e., $Q\tilde{\mathcal{L}}$ is Hermitian) and, hence, we consider the auxiliary Hermitian eigenvalue problem

$$Q(H_0 + \lambda H_I + mI) |k\rangle = E_k(m) |k\rangle, \quad (8)$$

or, equivalently, $(H_0 + \lambda H_I) |k\rangle = -m |k\rangle + E_k(m)Q |k\rangle$, where we used the fact that we are in the sector with $S = Q^2 = +1$. It follows that $-m$ is a real eigenvalue of the SYK Lindbladian when $E_k(m) = 0$ and, conversely, every real eigenvalue of \mathcal{L} corresponds to an intersection of some flow line $E_k(m)$ with the m -axis.

The number of intersections of the flow lines with the m -axis, weighted by the sign of the slope at the intersection, is a topological invariant W [41]

$$W = \sum_{k,\ell} \delta(m - m_k^{(\ell)}) \text{sign} \frac{dE_k(m)}{dm} = \int dm \frac{d}{dm} \text{sign}(E_k(m)), \quad (9)$$

where $m_k^{(\ell)}$ is the ℓ th intersection point of the flow line $E_k(m)$ with the m -axis. (Alternative integral representations for W exist [54].) W depends only on $E_k(m)$ evaluated at the endpoints $m \rightarrow \pm\infty$ and, in particular, is independent from λ . This follows immediately by evaluating the r.h.s. of Eq. (9) because, for $|m| \rightarrow \infty$, the eigenvalues of $Q\tilde{\mathcal{L}}$ approach the eigenvalues of Q . Since in the sector $Q^2 = S = +1$, Q has eigenvalues ± 1 , we obtain

$$W = \text{Tr } \mathbb{P}Q \equiv \nu(N, r), \quad (10)$$

where \mathbb{P} is the projector onto the relevant sector and the value of the topological index $\nu(N, r)$ is given in Table I.

It is instructive to compute W explicitly for $m = 0$. Since each intersection point of $E_k(m)$ with the real axis corresponds to a real eigenvalue of $Q\tilde{\mathcal{L}}$, we can write

$$W = \sum_{\{k|E_k=0\}} \text{sign} \frac{dE_k(m)}{dm}. \quad (11)$$

To proceed, we compute dE_k/dm by applying $\langle k|$ on the right of Eq. (8), and taking a derivative with respect to

m . Then we insert the corresponding result back into Eq. (11), which yields

$$W = \sum_{\{k|E_k=0\}} \text{sign} \langle k|Q|k \rangle. \quad (12)$$

For $\lambda = 0$, $\{H_0, Q\} = 0$, and in a chiral basis $Q|k\rangle = \pm|k\rangle$, where $Q = \text{diag}(\underbrace{1, \dots, 1}_{n+\nu}, \underbrace{-1, \dots, -1}_n)$. In this basis

the Hamiltonian H_0 has a chiral block structure with $(n+\nu) \times (n+\nu)$ and $n \times n$ blocks of zeros on the diagonal. We also have that $\zeta \langle k|Q|k \rangle = \langle k|\mathcal{L}Q|k \rangle = -\langle k|Q\mathcal{L}|k \rangle = -\zeta \langle k|Q|k \rangle$, where ζ are the eigenvalues of \mathcal{L} , so that $\langle k|Q|k \rangle$ vanishes unless $\zeta = 0$. We can, therefore, replace $\text{sign} \langle k|Q|k \rangle$ in Eq. (12) by $\langle k|Q|k \rangle$, and extend the sum of to all eigenstates $|k\rangle$ to arrive at Eq. (10).

The number of real eigenvalues is at least equal to, and can be larger than, the difference of the number of flow lines from $-\infty$ to $+\infty$ and from $+\infty$ to $-\infty$. A true crossing at $\lambda = 0$ can be deformed continuously into two lines with avoided crossings, resulting in two less real eigenvalues as m goes from $-\infty$ to $+\infty$. The number of real eigenvalues can change by a multiple of two when there are additional crossings. For example, if there are $2n$ additional crossings, it changes by $2n$, corresponding to n complex-conjugated pairs of eigenvalues entering the real line.

We have seen that the topological index W is equal to the analytic index $\text{Tr} \mathbb{P}Q$, which in our setting is closely related to the total number of real modes in the small- λ limit and, in turn, coincides with the parameter ν that controls the rectangularity of the block structure of \mathcal{L} . This is our main finding. In the next section, we present numerical results that illustrate our result, including the independence of W from λ . We stress that the existence of this topological invariant is an emergent property, due to an anomalous trace of the pseudo-Hermiticity operator, that cannot be easily guessed from the initial Liouvillian.

IV. NUMERICAL CALCULATION OF THE TOPOLOGICAL INDEX

We now confirm these results by an explicit calculation of the topological index from the spectral flow. In Fig. 1, we depict the m dependence of the eigenvalues $E_k(m)$, referred to as the spectral flow, when λ is small for the four universality classes with expected topological features, see Table I. Black (blue) curves contribute (do not contribute) to the topological index. With m going from $-\infty$ to $+\infty$, a line contributes $+1$ to the topological index W if the corresponding eigenvalue $E_k(m)$ runs from $-\infty$ to $+\infty$, and -1 if m goes from $+\infty$ to $-\infty$. In all cases, we have found agreement with the theoretical value of W , Eq. (10), which confirms the topological nature of the dynamics of our model. The spectral flow has a quite rich structure (especially for BDI_ν^\dagger and $\text{BDI}_{++\nu}$),

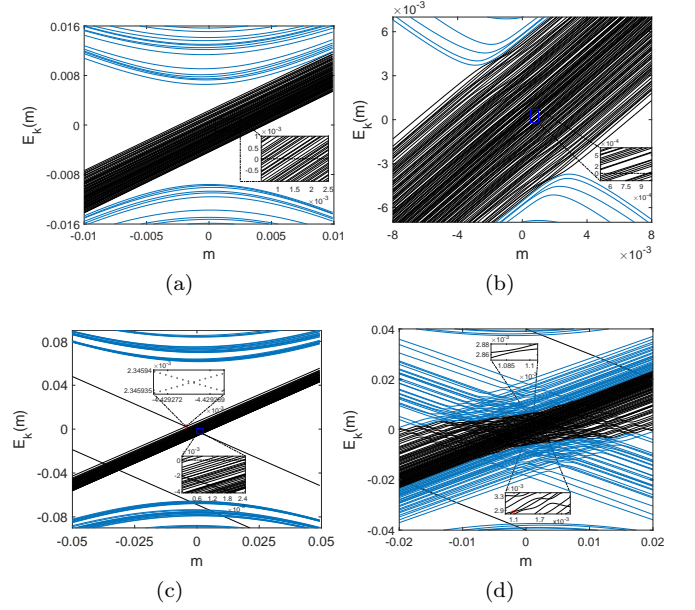


Figure 1. Spectral flow lines of the eigenvalues $E_k(m)$ of $Q\tilde{\mathcal{L}}$, where k labels the different eigenvalues. The blue and black curves denote spectral flow lines $E_k(m)$ with zero and ± 1 contributions to the topological index, respectively. (a) Class AIII_ν ; $N = 14, q = 4, r = 2, \lambda = 0.1, S_+ = S_- = -1$. Only $\nu = 32$ straight lines with positive slope contribute to the topological index. (b) Class $\text{CI}_{-\nu}$; $N = 14, q = 4, r = 1, \lambda = 0.01, S = 1$. We have found $W = \nu = 128$ flow lines going from $-\infty$ to $+\infty$. (c) Class BDI_ν^\dagger ; $N = 12, q = 4, r = 2, \lambda = 0.1, S_+ = S_- = -1$. There exist 48 flow lines that contribute $+1$ to the topological index, and 16 spectral flow lines (one that is 15-fold degenerate) that contribute with -1 , resulting in $W = \nu = 32$. As shown in the upper inset, the flow lines with a negative contribution to ν , which are analytical many-body scars [74], have true crossings with other flow lines. (d) Class $\text{BDI}_{++\nu}$; $N = 12, q = 4, r = 1, \lambda = 0.02, S = 1$. Despite a larger number of real modes than expected, as shown in Fig. 2 (left), the topological index is still the expected one, $W = \nu = 64$, with 68 and 4 flow lines contributing $+1$ and -1 to the topological index respectively. As is observed in both insets (note the difference of scale), many of the observed crossings are actually avoided crossings that do not contribute to the index.

that deserves further analysis.

For classes AIII_ν and $\text{CI}_{-\nu}$, see Fig. 1(a) and (b), the lines contributing to W are easily distinguished because they are also close to straight and run from $-\infty$ to $+\infty$ as a function of m , and each contributes $+1$ to W . By contrast, the pattern of the spectral flow for BDI_ν^\dagger at $N = 12$, Fig. 1(c), and $\text{BDI}_{++\nu}$ at $N = 12$, Fig. 1(d), is different, in part due to Kramers degeneracy in the spectrum for $\lambda = 0$.

For BDI_ν^\dagger and $N = 12$, due to this double degeneracy, we expect 64 real modes for not too large λ , 48 corresponding to flow lines from $-\infty$ to $+\infty$ and 16 corresponding to flow lines from $+\infty$ to $-\infty$. Therefore, by

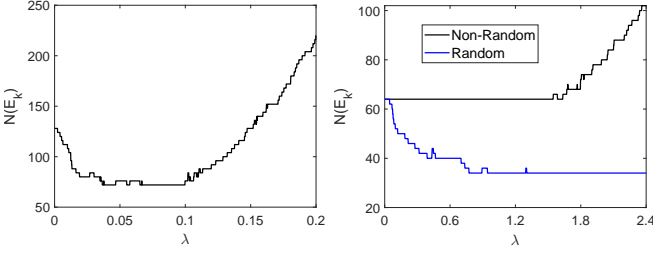


Figure 2. Number of exactly real modes as a function of λ for a single disorder realization for class $\text{BDI}_{++\nu}$ and $\text{BDI}_{\nu}^{\dagger}$. (Left) Class $\text{BDI}_{++\nu}$; $N = 12$, $q = 4$, $r = 1$, $S_+ = 1$. As theoretically expected, since H_I explicitly breaks the Kramers degeneracy, the number of exact real modes starts to decrease as λ increases. For $\lambda \in [0.04, 0.1]$, only 72 topological modes remain in most disorder realizations. (Right) Class $\text{BDI}_{\nu}^{\dagger}$; $N = 12$, $q = 4$, $r = 2$, $S_+ = S_- = 1$. Black: Contrary to the *naive* theoretical prediction that only half of the eigenvalues are topological, so that they should not stay on the real axis as λ increases, the number of real modes is independent of $\lambda < 2$. Blue: The same but considering a modified H_I Eq. (4) with Gaussian random couplings of zero mean and unit standard deviation. We observe the anticipated sharp decrease for small λ . The value of the plateau at intermediate λ coincides with the number of topological modes ($= 34$).

increasing λ , we expect the initial 64 real modes will reduce to only 32, until their number starts increasing again at a much larger value of λ due to additional crossings of the flow lines with the m -axis. Indeed, see Fig. 1(c), $W = \text{Tr } \mathbb{P}Q = \nu = 32$, but the form of the spectral flow is not exactly the expected one. One of the two lines in the spectral flow of Fig. 1(c), going from $+\infty$ to $-\infty$, has a fifteen fold degeneracy. Since there are 48 flow lines from $-\infty$ to $+\infty$, the topological index $W = 48 - 16 = 32$ agrees with the theoretical expectation. Intriguingly, as depicted in the right panel of Fig. 2, the number of real eigenvalues stays the same as λ increases. Only for large values of $\lambda > 1$, do we observe the expected increase of the number of real eigenvalues, not related to topology, but due to additional intersections of the flow lines. The reason for this unexpected behavior is that all sixteen flow lines with a negative contribution to the topological index are related to states that can be obtained analytically or semi-analytically, reminiscent of many-body scars [74]. As a consequence of a symmetry particular of H_I , these eigenvalues stay on the real axis as λ increases. Indeed, by considering the same H_I but with random couplings in Eq. (4), which does not alter the symmetry of the full Hamiltonian, we observe, see the right panel of Fig. 2, the anticipated quick decrease of the number of real modes as the coupling to the bath increases. Moreover, see Fig. 3, the spectral flow has the expected 32 lines from $-\infty$ to $+\infty$, though for some disorder realizations of H_I we still observe a single flow line with no degeneracy and a negative contribution to the topological index that also seems to correspond to a many-body scar.

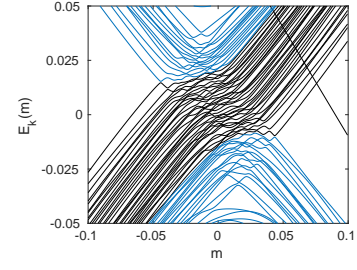


Figure 3. Spectral flow of $E_k(m)$, Eq. (8), for class $\text{BDI}_{\nu}^{\dagger}$ ($N = 12$, $q = 4$, $r = 2$, $\lambda = 1$, $S_+ = S_- = 1$), after introducing Gaussian random couplings with zero mean and unit standard deviation in H_I , Eq. (4). We find 33 lines with a positive contribution to ν and one line with a negative contribution which experiences an exact crossing with other flow lines, so that $W = 32 = \nu$.

For the $\text{BDI}_{++\nu}$ class, we observe the presence of many almost-straight flow lines from $-\infty$ to $+\infty$ but also from $+\infty$ to $-\infty$ contributing with $+1$ and -1 , respectively, leading ultimately to the expected topological index $W = 64 = \nu$. A substantial part of these flow lines do not contribute at all to the topological index because, after using a much finer resolution, we find most of the crossings are in fact avoided crossings, see insets of Fig. 1(d). Thus, each of these spectral lines flows from $+\infty$ to $+\infty$ or from $-\infty$ to $-\infty$, and do not contribute to the topological index. As mentioned before, the origin of the two types of flow lines is the Kramers degeneracy at $\lambda = 0$. As a result, the number of zero modes at $\lambda = 0$ is 128 with 96 flow lines from $-\infty$ to $+\infty$ and 32 flow lines from $+\infty$ to $-\infty$ resulting in an index of $\nu = 64$. For λ very small, most of the zero modes will stay real. However, only the difference of the two kinds of flow lines is topologically protected so, as λ increases, more real eigenvalues become complex until a minimum of 72 topologically protected real eigenvalues, 68 (4) with a positive (negative) contribution to the topological index, is reached, see left panel of Fig. 2. We note that the four modes with a negative contribution are, as in the $\text{BDI}_{\nu}^{\dagger}$ case, many-body scars located at $E_k(0) = \pm 2\lambda, \pm 6\lambda$.

Finally, we provide evidence that topology is restricted to classes for which $\text{Tr } \mathbb{P}_S^s Q$ is nonzero, which only happens for $s = +1$. For that purpose, we consider the cases where, for each realization, two symmetry classes, indexed by $S = \pm 1$, coexist in the same system. An example is $N/2$ odd and $q/2$ and r even. The $S = 1$ block has $\text{CI}_{-\nu}$ symmetry with $\nu = 2^{N/2}$ while the $S = -1$ block has BDI_{+} symmetry with $\nu = 0$. The spectral flow in the $S = +1$ sector was obtained in Fig. 1(d). In the $S = -1$ block, $\mathbb{P}_S^{-1} Q \mathcal{L}$ has purely imaginary eigenvalues, so we consider instead the spectral flow of $i\mathbb{P}_S^{-1} Q \mathcal{L}$, for $N = 10$, $q = 4$, $r = 2$, $S = -1$, see Fig. 4. It is fully symmetric with respect to the y-axis. The number of flow lines from $-\infty$ to $+\infty$ is equal to the number of flow lines from $+\infty$ to $-\infty$ resulting in a vanishing topological index. In the central part, $m \approx 0$, as shown in the

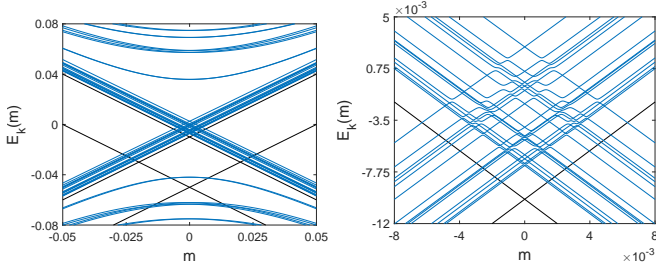


Figure 4. Spectral flow of $E_k(m)$, Eq. (8), for class BDI_{-+} ; $N = 10$, $q = 4$, $r = 1$, $\lambda = 0.01$, $S = -1$, and $m \in [-0.05, 0.05]$ (left) or $m \in [-0.008, 0.008]$ (right). The topological index is $W = 0$. Although superficially it seems that *straight* flow lines in the left panel contribute to W Eq. (10), at a finer scale (right), many of them show avoided crossings. Moreover, $E_k(m)$ is exactly symmetric around $E_k(0)$ so the topological index is zero.

right panel of Fig. 4, there are only avoided crossings so that the topological index of each line is actually zero.

V. UNIVERSALITY OF TOPOLOGY

Having provided convincing evidence of the topological nature of the real modes for certain universality classes of the SYK model coupled to a bath, we now turn to the discussion of the robustness and the universality of these results in different realms.

A. Topology and large λ

We expect that increasing λ does not affect the topological index as the eigenvalues are continuous functions of m and λ . As an example, the spectral flow in Fig. 5 for class CI_{-}^{ν} is quite different for $\lambda = 0.02$ and 0.08 but, of course, we still obtain the same topological index ν . The pattern for $\lambda = 0.08$ is much more intricate, with flow lines that may cross the m -axis many times while almost straight lines — typical for $\lambda = 0.02$ — are missing. Moreover, as can be deduced from the number of crossings of the flow lines with the m -axis, the number of purely real eigenvalues for $\lambda = 0.08$ has increased with respect to $\lambda = 0.02$, which may lead to the suspicion that the topological index has changed. However, this is not the case. As expected, we still find that $W = \nu$ for *every* disorder realization. This is a further confirmation that ν is a topological invariant independent on the total number of real modes or the coupling λ .

B. Dynamical generators beyond the Lindblad form

It is also clear from the symmetry classification in Table I that topology depends only on $r \bmod 2$ and N

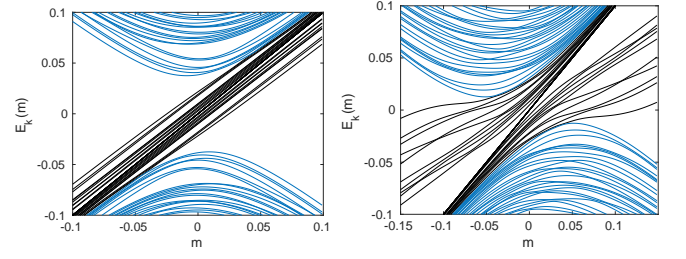


Figure 5. Spectral flow of $E_k(m)$, Eq. (8), for class CI_{-}^{ν} ; $N = 10$, $q = 4$, $r = 1$, $S = 1$, and $\lambda = 0.02$ (left) or $\lambda = 0.08$ (right). Despite the much more intricate pattern for $\lambda = 0.08$, $W = 32 = \nu$ [Eq. (10)] in both cases.

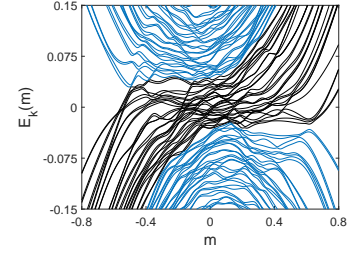


Figure 6. Spectral flow of $E_k(m)$, Eq. (8), considering a single-site SYK model Eq. (1) with both real and imaginary random couplings of the same strength ($\kappa = 1/2$), for $N = 10$, $q = 4$, $r = 1$, $\lambda = 0.01$, and $S = 1$. Although the corresponding symmetry class changes from CI_{-}^{ν} to $\text{BDI}_{\nu}^{\dagger}$, the topological index is still the same, $W = 32$, as in the case of purely real random coupling considered in the rest of the paper.

mod 4, so perturbations that remain in a given topological class will lead to an identical topological invariant $W = \nu$. Likewise, the presence of topology is insensitive to the addition of a purely real random part to the imaginary random couplings in Eq. (1), $iK_{i_1 \dots i_q} \rightarrow \sqrt{1 - \kappa}J_{i_1 \dots i_q} + i\sqrt{\kappa}K_{i_1 \dots i_q}$, with $\kappa \in [0, 1]$ parameterizing the degree of non-Hermiticity of the couplings [73], provided that the pseudo-Hermiticity of \mathcal{L} in Eq. (3) is preserved though the RMT symmetric class could change. Results for the spectral flow for $\kappa = 1/2$, depicted in Fig. 6, confirm the robustness of topology in this case. We note this addition of random real couplings corresponds to considering dissipative dynamics that, contrary to Lindbladian dynamics, do not preserve the trace of the density matrix. In Ref. [73], we recently showed that such dynamical generators can be mapped to PT-symmetric Hamiltonians and, therefore, also those non-Hermitian systems display topological behavior.

C. Non-SYK Lindbladians

We also explore whether topology is particular to the SYK setting by computing, see Fig. 7, the spectral flow associated to \mathcal{L} Eq. (3) after replacing the SYK model in class $\text{BDI}_{++\nu}$ with a spin chain in the same symmetry

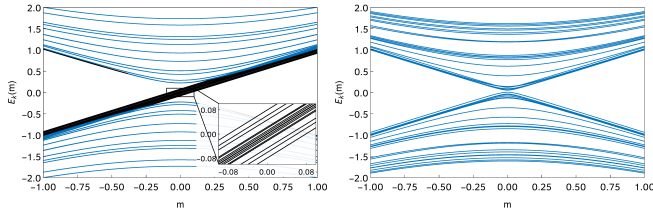


Figure 7. Spectral flow of $E_k(m)$, Eq. (8), for the dephasing spin chain of Ref. [75] with $L = 4$ and dissipation strength γ from a box distribution in $[0.005, 0.015]$. Left: Even parity sector, corresponding to class $\text{BDI}_{++\nu}$. The pseudo Hermiticity operator SWAP develops an anomalous trace ($\nu = 16$) which matches the topological index W , namely, there are exactly $W = \nu = 16$ lines flowing from $-\infty$ to $+\infty$. Right: Odd parity sector, corresponding to class CI_{+-} . SWAP is not anomalous and there are no signatures of topology in the spectral flow.

class. More precisely, we consider the XYZ spin chain in a transverse field and subject to dephasing defined in Eqs. (63), (64), (74), and (75) of Ref. [75] which we find belonging to class $\text{BDI}_{++\nu}$ (an exhaustive symmetry classification of such spin chains was provided in Ref. [75] but their topological nature was not identified). We use the same parameters as in Ref. [75], except that the chain length is $L = 4$ and we go to the weakly-dissipative regime (equivalent to small λ in the SYK setting), sampling the dephasing strength γ from a box distribution in $[0.005, 0.015]$. The pseudo-Hermiticity operator (equivalent to Q in SYK) is the SWAP operator defined as $\text{SWAP}(A \otimes B)\text{SWAP} = B \otimes A$ for any operators A and B , i.e., $\text{SWAP}\mathcal{L} = \mathcal{L}^\dagger\text{SWAP}$. In the even parity sector, SWAP develops an anomalous trace $\nu = 2^L$ and, computing the spectral flow, we find, as expected, the topological index $W = \nu = 2^L$.

In fact, the mechanism for the emergence of topology is the existence of a pseudo-Hermiticity operator with anomalous trace. In Lindbladian systems, the operator exchanging the bra and ket spaces of the density matrix (or Keldysh contours) is the most natural candidate, as we demonstrated explicitly for the SYK model and spin chains. Therefore, it is likely that the only necessary ingredients for topology (besides anomalous pseudo-Hermiticity) are that the Lindbladian does not break up in finer blocks, which is the case if the system is quantum chaotic. However, more work is needed to settle this issue.

D. Dynamical and experimental signatures

A major appeal of topology is its experimental relevance. For instance, in systems experiencing the integer or spin Hall effect, linear response transport is governed by a topological invariant. By contrast, topology in the vectorized SYK Liouvillian Eq. (3) reveals itself in the full out-of-equilibrium time evolution. Indeed, the topo-

logical real modes have a sharp dynamical interpretation. These modes control the approach to a steady of the system independently of the coupling to the bath λ provided that it is weak enough so that all real modes are topological. A promising computational scheme to reveal these topological features in the dynamics is that of subspace-Krylov techniques that may allow reach a N sufficiently large to compare with the non-topological saddle-point results for the decay rate [70]. A direct experimental measure of the decay rate by using quantum optical settings [36] with the appropriate symmetry is also feasible.

E. Topology and level statistics of real modes

We now turn to another playground to probe topology: level statistics. We have recently found [45, 53, 73] that, perturbatively ($\lambda \ll 1$), level statistics of the topological real modes for classes AIII_ν , BDI_ν^\dagger , $\text{CI}_{-\nu}$ and $\text{BDI}_{++\nu}$ are given by those of random Hermitian matrices belonging to the GUE, GOE, CI, and BDI universality classes respectively. In this section, we test the robustness of these results in our SYK setting.

We first consider $\text{CI}_{-\nu}$ at $N = 14$, corresponding to $q = 4$, $r = 1$ where, for small λ , the number of exact real modes is equal to the number of topological modes. In that case, we have found, both in the bulk — by the calculation of the distribution of the gap ratio $P(r)$ [76] — and close to the origin — where we compute the microscopic spectral density $\rho_M(E)$ — an excellent agreement with the RMT prediction for class CI, see Fig. 8 (left). Also for class AIII_ν , all real eigenvalues are topological for not very large λ and we find (not shown) a very similar level of agreement with the predicted GUE class [73].

As mentioned earlier, the situation is more complicated for $\text{BDI}_{++\nu}$. Due to the Kramers degeneracy at $\lambda = 0$, for sufficiently small λ , the number of topological modes is only about half the total number of real modes, see left plot of Fig. 2. Therefore, we expect deviations from the RMT prediction for small λ and find agreement once the number of real eigenvalues is equal to $\nu = \text{Tr } \mathbb{P}Q$.

The results depicted in Fig. 8 (right) largely confirm this picture. In the bulk of the spectrum, $P(r)$ deviates strongly from the BDI prediction (i.e., GOE statistics) for very small λ . The agreement with BDI gradually improves as λ increases and most real eigenvalues correspond to flow lines that intersect the m -axis only once. Similar level of agreement occurs for the microscopic spectral density $\rho_M(E)$, namely, there is good agreement with the random matrix result in class BDI, provided that the number of real modes is close to ν .

The remaining class, BDI_ν^\dagger , also has Kramers degeneracy, so superficially one would expect similar deviations as in the $\text{BDI}_{++\nu}$ class. However, $P(r)$, depicted in the left panel of Fig. 9, shows excellent agreement with the predicted GOE result for a broad range of values of λ . Moreover, unlike the $\text{BDI}_{++\nu}$ class, the number of real modes, see left plot of Fig. 2, does not depend on λ un-

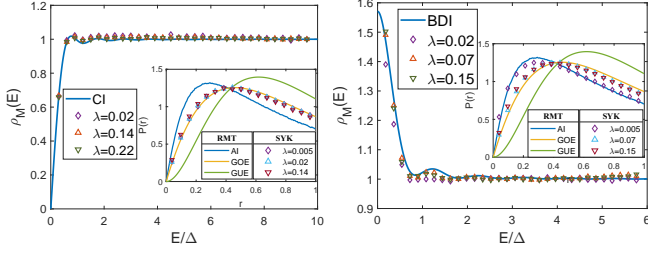


Figure 8. Left: Level statistics for the real modes of \mathcal{L} Eq. (3) for class $\text{CI}_{-,\nu}$ with $N = 14$, $q = 4$, $r = 1$, $S = 1$, and 2.5×10^5 realizations. Microscopic spectral density $\rho_M(E)$ of the real modes close to $E = 0$ in units of the meal level spacing Δ . Inset: Distribution of the gap ratio $P(r)$ with 10^4 realizations in the bulk of the spectrum. We observe excellent agreement with the CI random matrix results for all λ . Right: Level statistics of the real modes of \mathcal{L} Eq. (3) for class $\text{BDI}_{+,\nu}$ with $N = 12$, $q = 4$, $r = 1$, $S = 1$, and 10^6 realizations. $\rho_M(E)$ shows good agreement with the BDI random matrix prediction for λ corresponding to the region where most real eigenvalues are topological. Inset: Distribution of the gap ratio $P(r)$ with 4×10^4 realizations in the bulk of the spectrum which shows good agreement with RMT in the expected region of parameters. From Fig. 2 (left), $\lambda = 0.07$ is located at the plateau stage. We choose all 4×10^4 realizations from the ones where all purely real modes are topological (in total 72).

less it is very large ($\lambda > 2$), and the direct effect of the bath pushes eigenvalues onto the real axis. The origin of this unexpected behavior is the existence of two real modes, one with a fifteen fold degeneracy, that do not enter in the level statistics calculation because they seem to be related to many-body scars [74] and therefore are not quantum chaotic. The degenerate flow lines with negative slope have exact crossings with the flow lines with a positive slope and cannot be deformed into pairs of flow lines that do not intersect the m -axis. Therefore, even though there are more real modes than the value of the topological index, all eigenvalues included in the level statistics analysis are topological (i.e. intersect the m -axis only once), so the observed agreement with the GOE class is not unexpected.

As a confirmation of this point, we repeat the calculation of $P(r)$ for random couplings in H_I , Eq. (4), so that the symmetry is still BDI_ν^\dagger . In this case, the dependence on the number of real modes with λ , see right panel of Fig. 2, is very similar to that of the $\text{BDI}_{+,\nu}$ class. Not surprisingly, the λ dependence of $P(r)$, see right panel of Fig. 9, mimics that of the $\text{BDI}_{+,\nu}$ class. The slightly larger deviation for intermediate λ values may be due to the single mode related to scars that are included in the level statistics analysis.

These results point to a nuanced relation between topology and level statistics if not all real modes are topological as in $\text{BDI}_{+,\nu}$ and BDI_ν^\dagger classes. Therefore, a symmetry classification of many-body non-Hermitian topology by level statistics is feasible but likely will require

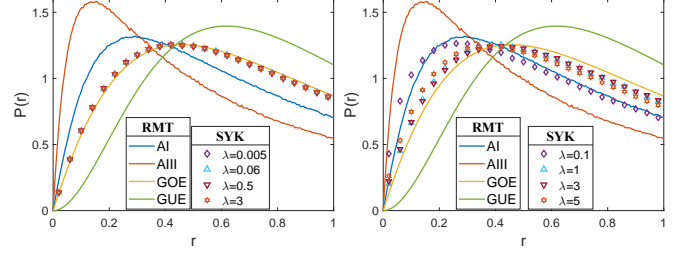


Figure 9. Left: $P(r)$ for the bulk real eigenmodes of \mathcal{L} Eq. (3) with $N = 12$, $q = 4$, $r = 2$, and 8×10^4 corresponding to class BDI_ν^\dagger . We find excellent agreement with the BDI random matrix prediction as all real eigenvalues are topological. We note that the sixteen eigenvalues with a negative contribution to ν are related to many-body scars, and therefore are excluded from the level statistics analysis. Right: Same parameters as in the left plot but using random couplings in H_I , Eq. (4). For $\lambda = 1, 3$ in the plateau region, as shown in Fig. 2 (right), we only choose the 8×10^4 realizations from those with only 34 topological modes. When the value of λ is such that the number of real modes approaches ν , the agreement with the GOE prediction improves. The remaining deviations for intermediate values of λ may be due to the effect of a single eigenvalue, related to a many-body scar, that is included in the level statistics analysis.

extra effort to identify topology just by a level statistics analysis.

VI. CONCLUSION AND OUTLOOK

For four pseudo-Hermitian symmetry classes, AIII_ν , BDI_ν^\dagger , $\text{CI}_{-,\nu}$, and $\text{BDI}_{+,\nu}$ [73], we have found robust topological features in the dynamics of a single site SYK weakly coupled to a Markovian bath which is a paradigmatic model of dissipative many-body quantum chaos. The route to recognizing topology in this setting starts with the observation that the trace of the projection of a unitary operator Q , related to the pseudo-Hermiticity of the vectorized Liouvillian, is non-vanishing. Specifically, after projection onto states with even parity, Q develops an anomalous trace, $\text{Tr } \mathbb{P}Q = \nu \neq 0$. As is the case for the Dirac operator for gauge fields with a nonzero topological charge, in the limit of zero coupling, the vectorized Liouvillian admits a representation with diagonal blocks of zeros of unequal size leading to exact zero modes. For small λ , we have shown those zero modes become real modes of the Liouvillian. We stress that this rectangularity is an emergent property and is not introduced ad hoc.

Using spectral flow, we have shown, analytically and numerically, that for these four classes the index $\text{Tr } \mathbb{P}Q = \nu$ is a topological invariant that is stable with respect to deformations of the Liouvillian. The topological structure is also robust to the replacement of the SYK model by a spin chain with the same symmetry or to the addition of a non-Hermitian part to the single-site

SYK, which illustrates the universality of our results. Physically, the topological invariant can be interpreted as a pseudo-Hermiticity quantum anomaly, represented by the exchange operator Q , reminiscent of the chiral anomaly in QCD.

Topology leaves an imprint on the level statistics of real modes though the degree of universality is limited by the presence, in some cases, of real modes not related to topology. In the limit of weak coupling, these topological modes control the dynamics for late times. Therefore, anomalies in the decay rate to the steady state are fingerprints of topology. We stress our findings are unrelated with the physics of topological insulators or its non-Hermitian analogue since in our case interactions are crucial for the existence of topological states.

Natural extensions of our work include a full classification of topological universality classes, out of the 38 [33, 77] for non-Hermitian systems, and the effect of topology on equilibration. Generalizations to higher dimensions or the use of tensor [78–81] supersymmetric [82–85] or Wishart [86] SYK models are natural choices to

further explore topology in many-body dissipative quantum chaos.

ACKNOWLEDGMENTS

AMGG and YC were supported by NSFC Grant No. 11874259, the National Key R&D Program of China (Project ID: 2019YFA0308603), and a Shanghai talent program. LS acknowledges was supported by a Research Fellowship from the Royal Commission for the Exhibition of 1851 and by Fundação para a Ciência e a Tecnologia (FCT-Portugal) through Grant No. SFRH/BD/147477/2019. JJMV acknowledges support from U.S. DOE Grant No. DE-FAG88FR40388. LS and JJMV acknowledge hospitality and support from the Simons Center for Geometry and Physics and the program “Fluctuations, Entanglements, and Chaos: Exact Results”, where some of the ideas of this paper were developed.

* amgg@sjtu.edu.cn

† ld710@cam.ac.uk

‡ jacobus.verbaarschot@stonybrook.edu

§ yin_can@sjtu.edu.cn

- [1] S. L. Adler, Axial-Vector Vertex in Spinor Electrodynamics, *Phys. Rev.* **177**, 2426 (1969).
- [2] J. S. Bell and R. Jackiw, A PCAC puzzle: $\pi^0 \rightarrow \gamma\gamma$ in the σ model, *Nuovo Cim. A* **60**, 47 (1969).
- [3] G. 't Hooft, Computation of the quantum effects due to a four-dimensional pseudoparticle, *Phys. Rev. D* **14**, 3432 (1976).
- [4] N. Nielsen and B. Schroer, Axial anomaly and Atiyah-Singer theorem, *Nucl. Phys. B* **127**, 493 (1977).
- [5] M. F. Atiyah and I. M. Singer, The Index of Elliptic Operators: I, *Ann. Math.* **87**, 484 (1968).
- [6] E. Shuryak, The role of instantons in quantum chromodynamics: (I). Physical vacuum, *Nucl. Phys. B* **203**, 93 (1982).
- [7] J. J. M. Verbaarschot and I. Zahed, Spectral density of the QCD Dirac operator near zero virtuality, *Phys. Rev. Lett.* **70**, 3852 (1993).
- [8] J. Verbaarschot, Spectrum of the QCD Dirac operator and chiral random matrix theory, *Phys. Rev. Lett.* **72**, 2531 (1994).
- [9] K. v. Klitzing, G. Dorda, and M. Pepper, New Method for High-Accuracy Determination of the Fine-Structure Constant Based on Quantized Hall Resistance, *Phys. Rev. Lett.* **45**, 494 (1980).
- [10] D. J. Thouless, M. Kohmoto, M. P. Nightingale, and M. den Nijs, Quantized Hall Conductance in a Two-Dimensional Periodic Potential, *Phys. Rev. Lett.* **49**, 405 (1982).
- [11] D. C. Tsui, H. L. Stormer, and A. C. Gossard, Two-Dimensional Magnetotransport in the Extreme Quantum Limit, *Phys. Rev. Lett.* **48**, 1559 (1982).
- [12] R. B. Laughlin, Anomalous Quantum Hall Effect: An Incompressible Quantum Fluid with Fractionally Charged Excitations, *Phys. Rev. Lett.* **50**, 1395 (1983).
- [13] F. D. M. Haldane, Model for a Quantum Hall Effect without Landau Levels: Condensed-Matter Realization of the "Parity Anomaly", *Phys. Rev. Lett.* **61**, 2015 (1988).
- [14] M. König, S. Wiedmann, C. Brune, A. Roth, H. Buhmann, L. W. Molenkamp, X.-L. Qi, and S.-C. Zhang, Quantum Spin Hall Insulator State in HgTe Quantum Wells, *Science* **318**, 766 (2007).
- [15] C. L. Kane and E. J. Mele, Quantum Spin Hall Effect in Graphene, *Phys. Rev. Lett.* **95**, 226801 (2005).
- [16] C. L. Kane and E. J. Mele, Z_2 Topological Order and the Quantum Spin Hall Effect, *Phys. Rev. Lett.* **95**, 146802 (2005).
- [17] B. A. Bernevig, T. L. Hughes, and S.-C. Zhang, Quantum Spin Hall Effect and Topological Phase Transition in HgTe Quantum Wells, *Science* **314**, 1757 (2006).
- [18] L. Fu, C. L. Kane, and E. J. Mele, Topological Insulators in Three Dimensions, *Phys. Rev. Lett.* **98**, 106803 (2007).
- [19] L. Fu and C. L. Kane, Topological insulators with inversion symmetry, *Phys. Rev. B* **76**, 045302 (2007).
- [20] R. Roy, Topological phases and the quantum spin Hall effect in three dimensions, *Phys. Rev. B* **79**, 195322 (2009).
- [21] J. E. Moore and L. Balents, Topological invariants of time-reversal-invariant band structures, *Phys. Rev. B* **75**, 121306(R) (2007).
- [22] D. Hsieh, D. Qian, L. Wray, Y. Xia, Y. S. Hor, R. J. Cava, and M. Z. Hasan, A topological Dirac insulator in a quantum spin Hall phase, *Nature* **452**, 970 (2008).
- [23] M. Sato and Y. Ando, Topological superconductors: a review, *Rep. Prog. Phys.* **80**, 076501 (2017).
- [24] A. Kitaev, Periodic table for topological insulators and superconductors, *AIP Conf. Proc.* **1134**, 22 (2009).
- [25] S. Ryu, A. P. Schnyder, A. Furusaki, and A. W. W. Ludwig, Topological insulators and superconductors: tenfold way and dimensional hierarchy, *New J. Phys.* **12**, 065010 (2010).

- [26] A. P. Schnyder, S. Ryu, A. Furusaki, and A. W. W. Ludwig, Classification of topological insulators and superconductors in three spatial dimensions, *Phys. Rev. B* **78**, 195125 (2008).
- [27] L. Fidkowski and A. Kitaev, Effects of interactions on the topological classification of free fermion systems, *Phys. Rev. B* **81**, 134509 (2010).
- [28] K. Esaki, M. Sato, K. Hasebe, and M. Kohmoto, Edge states and topological phases in non-Hermitian systems, *Phys. Rev. B* **84**, 205128 (2011).
- [29] M. S. Rudner and L. S. Levitov, Topological Transition in a Non-Hermitian Quantum Walk, *Phys. Rev. Lett.* **102**, 065703 (2009).
- [30] Y. C. Hu and T. L. Hughes, Absence of topological insulator phases in non-Hermitian PT -symmetric Hamiltonians, *Phys. Rev. B* **84**, 153101 (2011).
- [31] N. Okuma and M. Sato, Non-Hermitian Topological Phenomena: A Review, *Annu. Rev. Condens. Matt. Phys.* **14**, 83 (2023).
- [32] Z. Gong, Y. Ashida, K. Kawabata, K. Takasan, S. Higashikawa, and M. Ueda, Topological Phases of Non-Hermitian Systems, *Phys. Rev. X* **8**, 031079 (2018).
- [33] K. Kawabata, K. Shiozaki, M. Ueda, and M. Sato, Symmetry and Topology in Non-Hermitian Physics, *Phys. Rev. X* **9**, 041015 (2019).
- [34] H. Shen, B. Zhen, and L. Fu, Topological Band Theory for Non-Hermitian Hamiltonians, *Phys. Rev. Lett.* **120**, 146402 (2018).
- [35] S. Yao and Z. Wang, Edge States and Topological Invariants of Non-Hermitian Systems, *Phys. Rev. Lett.* **121**, 086803 (2018).
- [36] H. Schomerus, Topologically protected midgap states in complex photonic lattices, *Opt. Lett.* **38**, 1912 (2013).
- [37] F. K. Kunst, E. Edvardsson, J. C. Budich, and E. J. Bergholtz, Biorthogonal Bulk-Boundary Correspondence in Non-Hermitian Systems, *Phys. Rev. Lett.* **121**, 026808 (2018).
- [38] D. S. Borgnia, A. J. Kruchkov, and R.-J. Slager, Non-Hermitian Boundary Modes and Topology, *Phys. Rev. Lett.* **124**, 056802 (2020).
- [39] N. Okuma, K. Kawabata, K. Shiozaki, and M. Sato, Topological Origin of Non-Hermitian Skin Effects, *Phys. Rev. Lett.* **124**, 086801 (2020).
- [40] F. Schindler, K. Gu, B. Lian, and K. Kawabata, Hermitian Bulk – Non-Hermitian Boundary Correspondence, *PRX Quantum* **4**, 030315 (2023).
- [41] S. Itoh, Y. Iwasaki, and T. Yoshie, The $U(1)$ Problem and Topological Excitations on a Lattice, *Phys. Rev. D* **36**, 527 (1987).
- [42] M. F. L. Golterman, K. Jansen, and D. B. Kaplan, Chern-Simons currents and chiral fermions on the lattice, *Phys. Lett. B* **301**, 219 (1993).
- [43] R. Narayanan and H. Neuberger, A Construction of lattice chiral gauge theories, *Nucl. Phys. B* **443**, 305 (1995).
- [44] D. B. Kaplan, Chiral Symmetry and Lattice Fermions, in *Les Houches Summer School: Session 93: Modern perspectives in lattice QCD: Quantum field theory and high performance computing* (2009) pp. 223–272, [arXiv:0912.2560 \[hep-lat\]](https://arxiv.org/abs/0912.2560).
- [45] G. Akemann, P. H. Damgaard, K. Splittorff, and J. J. M. Verbaarschot, Spectrum of the Wilson Dirac Operator at Finite Lattice Spacings, *Phys. Rev. D* **83**, 085014 (2011).
- [46] J. C. Osborn, Universal results from an alternate random matrix model for QCD with a baryon chemical potential, *Phys. Rev. Lett.* **93**, 222001 (2004).
- [47] G. Akemann, J. C. Osborn, K. Splittorff, and J. J. M. Verbaarschot, Unquenched QCD Dirac operator spectra at nonzero baryon chemical potential, *Nucl. Phys. B* **712**, 287 (2005).
- [48] T. Kanazawa, T. Wettig, and N. Yamamoto, Chiral random matrix theory for two-color QCD at high density, *Phys. Rev. D* **81**, 081701(R) (2010).
- [49] P. H. Damgaard, K. Splittorff, and J. J. M. Verbaarschot, Microscopic Spectrum of the Wilson Dirac Operator, *Phys. Rev. Lett.* **105**, 162002 (2010).
- [50] M. Kieburg, J. J. M. Verbaarschot, and S. Zafeiropoulos, Eigenvalue Density of the non-Hermitian Wilson Dirac Operator, *Phys. Rev. Lett.* **108**, 022001 (2012).
- [51] G. Akemann and T. Nagao, Random matrix theory for the Hermitian Wilson Dirac operator and the chGUE-GUE transition, *J. High Energy Phys.* **10** (2011).
- [52] M. Kieburg, J. J. M. Verbaarschot, and S. Zafeiropoulos, Spectral properties of the Wilson Dirac operator and random matrix theory, *Phys. Rev. D* **88**, 094502 (2013).
- [53] M. Kieburg, J. J. M. Verbaarschot, and S. Zafeiropoulos, Dirac Spectrum of the Wilson Dirac Operator for QCD with Two Colors, *Phys. Rev. D* **92**, 045026 (2015).
- [54] K. Kawabata, K. Shiozaki, and S. Ryu, Many-body topology of non-Hermitian systems, *Phys. Rev. B* **105**, 165137 (2022).
- [55] S.-B. Zhang, M. M. Denner, T. Bzdušek, M. A. Sentef, and T. Neupert, Symmetry breaking and spectral structure of the interacting hatano-nelson model, *Phys. Rev. B* **106**, L121102 (2022).
- [56] N. Hatano and D. R. Nelson, Localization transitions in non-hermitian quantum mechanics, *Phys. Rev. Lett.* **77**, 570 (1996).
- [57] W. N. Fauson and T. Ozawa, Interaction-Induced Non-Hermitian Topological Phases from a Dynamical Gauge Field, *Phys. Rev. Lett.* **129**, 180401 (2022).
- [58] S. Hamanaka, K. Yamamoto, and T. Yoshida, Interaction-induced Liouvillian skin effect in a fermionic chain with a two-body loss, *Phys. Rev. B* **108**, 155114 (2023).
- [59] T. Yoshida and Y. Hatsugai, Fate of exceptional points under interactions: Reduction of topological classifications, *Phys. Rev. B* **107**, 075118 (2023).
- [60] O. Bohigas and J. Flores, Two-body random hamiltonian and level density, *Phys. Lett. B* **34**, 261 (1971).
- [61] J. French and S. Wong, Validity of random matrix theories for many-particle systems, *Phys. Lett. B* **33**, 449 (1970).
- [62] O. Bohigas and J. Flores, Spacing and individual eigenvalue distributions of two-body random hamiltonians, *Phys. Lett. B* **35**, 383 (1971).
- [63] J. B. French and S. S. M. Wong, Some random-matrix level and spacing distributions for fixed-particle-rank interactions, *Phys. Lett. B* **35**, 5 (1971).
- [64] K. Mon and J. French, Statistical properties of many-particle spectra, *Ann. Phys.* **95**, 90 (1975).
- [65] A. Kitaev, A simple model of quantum holography (2015), string seminar at KITP and Entanglement 2015 program, 12 February, 7 April and 27 May 2015, <http://online.kitp.ucsb.edu/online/entangled15/>.
- [66] J. Maldacena and D. Stanford, Remarks on the Sachdev-Ye-Kitaev model, *Phys. Rev. D* **94**, 106002 (2016).
- [67] L. Sá, P. Ribeiro, and T. Prosen, Lindbladian dissipation of strongly-correlated quantum matter, *Phys. Rev.*

- Research **4**, L022068 (2022).
- [68] A. Kulkarni, T. Numasawa, and S. Ryu, Lindbladian dynamics of the Sachdev-Ye-Kitaev model, *Phys. Rev. B* **106**, 075138 (2022).
 - [69] K. Kawabata, A. Kulkarni, J. Li, T. Numasawa, and S. Ryu, Dynamical quantum phase transitions in Sachdev-Ye-Kitaev Lindbladians, *Phys. Rev. B* **108**, 075110 (2023).
 - [70] A. M. García-García, L. Sá, J. J. M. Verbaarschot, and J. P. Zheng, Keldysh wormholes and anomalous relaxation in the dissipative Sachdev-Ye-Kitaev model, *Phys. Rev. D* **107**, 106006 (2023).
 - [71] H. Wang, C. Liu, P. Zhang, and A. M. García-García, Entanglement Transition and Replica Wormhole in the Dissipative Sachdev-Ye-Kitaev Model, [arXiv:2306.12571](#) (2023).
 - [72] K. Kawabata, A. Kulkarni, J. Li, T. Numasawa, and S. Ryu, Symmetry of Open Quantum Systems: Classification of Dissipative Quantum Chaos, *PRX Quantum* **4**, 030328 (2023).
 - [73] A. M. García-García, L. Sá, J. J. M. Verbaarschot, and C. Yin, Towards a classification of PT-symmetric quantum systems: from dissipative dynamics to topology and wormholes, [arXiv:2311.15677](#) (2023).
 - [74] C. J. Turner, A. A. Michailidis, D. A. Abanin, M. Serbyn, and Z. Papić, Weak ergodicity breaking from quantum many-body scars, *Nat. Phys.* **14**, 745–749 (2018).
 - [75] L. Sá, P. Ribeiro, and T. Prosen, Symmetry Classification of Many-Body Lindbladians: Tenfold Way and Beyond, *Phys. Rev. X* **13**, 031019 (2023).
 - [76] Y. Y. Atas, E. Bogomolny, O. Giraud, and G. Roux, Distribution of the Ratio of Consecutive Level Spacings in Random Matrix Ensembles, *Phys. Rev. Lett.* **110**, 084101 (2013).
 - [77] D. Bernard and A. LeClair, A classification of non-hermitian random matrices, in *Statistical Field Theories*, edited by M. G. Cappelletti A. (Springer, 2002) pp. 207–214, [arXiv:0110649](#).
 - [78] E. Witten, An SYK-Like Model Without Disorder, *J. Phys. A* **52**, 474002 (2019).
 - [79] R. Gurau, The complete $1/N$ expansion of a SYK-like tensor model, *Nucl. Phys. B* **916**, 386 (2017).
 - [80] C. Krishnan, S. Sanyal, and P. N. B. Subramanian, Quantum chaos and holographic tensor models, *Journal of High Energy Physics* **2017**, 56 (2017).
 - [81] J. Kim, I. R. Klebanov, G. Tarnopolsky, and W. Zhao, Symmetry Breaking in Coupled SYK or Tensor Models, *Phys. Rev. X* **9**, 021043 (2019).
 - [82] W. Fu, D. Gaiotto, J. Maldacena, and S. Sachdev, Supersymmetric Sachdev-Ye-Kitaev models, *Phys. Rev. D* **95**, 026009 (2017).
 - [83] T. Kanazawa and T. Wettig, Complete random matrix classification of SYK models with $\mathcal{N} = 0, 1$ and 2 supersymmetry, *J. High Energy Phys.* **9** (2017).
 - [84] A. M. García-García, Y. Jia, and J. J. M. Verbaarschot, Universality and Thouless energy in the supersymmetric Sachdev-Ye-Kitaev model, *Phys. Rev. D* **97**, 106003 (2018).
 - [85] T. Li, J. Liu, Y. Xin, and Y. Zhou, Supersymmetric SYK model and random matrix theory, *J. High Energy Phys.* **6** (2017).
 - [86] L. Sá and A. M. García-García, Q -Laguerre spectral density and quantum chaos in the Wishart-Sachdev-Ye-Kitaev model, *Phys. Rev. D* **105**, 026005 (2022).